EUROFUSION WPMAG-PR(16) 16527

N Bykovsky et al.

Magnetization loss for stacks of ReBCO tapes

Preprint of Paper to be submitted for publication in
Superconductor Science and Technology

This work has been carried out within the framework of the EUROfusion Consortium and has received funding from the Euratom research and training programme 2014-2018 under grant agreement No 633053. The views and opinions expressed herein do not necessarily reflect those of the European Commission.

Magnetization loss for stacks of ReBCO tapes

N. Bykovsky[1], G. De Marzi[2], D. Uglietti[1], P. Bruzzone[1] and L. Muzzi[2,3]

[1]EPFL-SPC, Superconductivity group, Villigen PSI, Switzerland
[2]ENEA–FSN, C. R. Frascati, Via Enrico Fermi 45, 00044 Frascati, Italy
[3]ICAS S.C.r.l., Frascati, Rome, Italy

E-mail: nikolay.bykovsky@psi.ch

Abstract. The AC loss measurements of the HTS cable prototype in the EDIPO test facility motivated detailed investigations of the loss contributions from the tape, strand and cable stages of the HTS fusion conductor design proposed at Swiss Plasma Center (SPC). As an initial step of the task, magnetization tests of soldered stacks of HTS tapes were carried out at 5 K and 77 K temperatures and magnetic fields up to 12 T using the vibrating sample magnetometer (VSM) technique. The influence on the magnetization loss of the number of tapes, width of the tape, field's orientation and tape's manufacturer is studied experimentally performing both the major and minor magnetization loops with different ramp rates of the applied magnetic field. In order to validate the test results, a numerical model is developed and presented in this work. From the numerical model we also deduced an analytical approach for the magnetization loss in the stacks of tapes with arbitrary number of tapes in the critical state model. Comparison between the measured and estimated magnetization loss of the cable prototypes is reported as well.

Keywords: coated conductors, stack of HTS tapes, magnetization, VSM, numerical model, AC losses

Submitted to: *Supercond. Sci. Technol.*

1. Introduction

Various DC and AC measurements were performed with the 60 kA HTS fusion cable prototype in the EDIPO test facility [1]. The test results have been published recently in [2, 3]. Though the prototype was not designed for low AC loss, one of the issues obtained from the EDIPO measurements is relatively high AC loss in time varying magnetic field. As a result, additional investigations started over different AC loss contributions related to the geometry of the cable concept proposed at SPC.

The task starts with a study of the magnetization loss of the stack of HTS tape. In order to provide a comprehensive view on the selected topic, various effects have been studied such as the influence of the number of tapes in the stack, width of tapes, orientation of the applied magnetic field and manufacturer of the HTS tape.

There are several approaches applicable for numerical analysis of the stack's magnetization – widely used FEM modeling [4, 5], integro-differential methods [6,

7], variational formulation [8, 9]. The latter one was justified for the effective solving of high complexity problems [10] and recently generalized to deal with a smooth transition of the current–voltage relation of the superconducting material [11]. The variational formulation has been selected for the numerical model.

A set of short samples is prepared, see section 3. Isothermal magnetization loops of the samples were measured using a vibrating sample magnetometer (VSM) equipped with a 12 T superconducting magnet and a variable temperature insert. The temperature of the sample can be varied by flowing He gas through a needle valve and by controlling with a PID feedback system. Measurements have been collected at 5 K and 77 K, in background magnetic field up to 12 T and different orientations of the samples: 0°, 45° and 90°, see section 4.

Using the data obtained from the numerical and experimental analyses, the magnetization loss of the stacks is assessed as a function of the various aspects of the stack, see section 5 together with the data from the HTS cable measurements in EDIPO.

2. Numerical modeling

2.1. Description of the model

A general variational approach for the electro-magnetic modeling of the superconductors with a smooth $E(J)$ relation was summarized in [11], where it was demonstrated that minimization of the certain scalar function L of multiple variables ('functional') is equivalent to solving the Maxwell equations. There are two options for the definition of L: magnetic field H and current density-scalar potential $J - \phi$ formulations. The latter one is selected for the stack's magnetization model since it only requires meshing over the superconductor domain. Eliminating the grid over 'air' allows speeding up the calculation.

Now, let locate the stack at the origin with c-axis along the vertical y direction and assume it infinitely long in the z direction. Hence we will consider only longitudinal currents in the stack induced by the external magnetic field and/or transport current. A sketch of the stack geometry used in the model is presented in figure 1. The superconducting layer of each tape in the stack is presented in the model as a thin rectangle with the width w and thickness $d = 1\,\mu\text{m}$. Considering n_t tapes in the stack and dividing each tape by N_x cells along the width, the total number of mesh elements in the model becomes $N = n_t \cdot N_x$. We use a uniform grid, so the width of each cell is $s = w/N_x$. The cells are centered at the positions (x_i, y_j): $x_i = s(i - (N_x + 1)/2)$, $y_j = D(j - (n_t + 1)/2)$ ($i = 1 \dots N_x$, $j = 1 \dots n_t$, D is the vertical distance between the mesh elements).

Implying zero background magnetic field and transport current at the initial time, the trivial solution for the current distribution in the stack is $I_k(t = 0) = 0$, $(k = 1 \dots N)$. Then, at the following time step Δt, the external magnetic field is increased by $\Delta\vec{B}_a$ at angle θ_a to the c-axis of the stack (i.e. $\Delta\vec{B}_a = \Delta B_a\{\cos\theta_a, \sin\theta_a, 0\}$), that corresponds to a change of the vector potential $\Delta\vec{A}_a = \{0, 0, (-x\cos\theta_a + y\sin\theta_a)\Delta B_a\}$ in Coulomb's

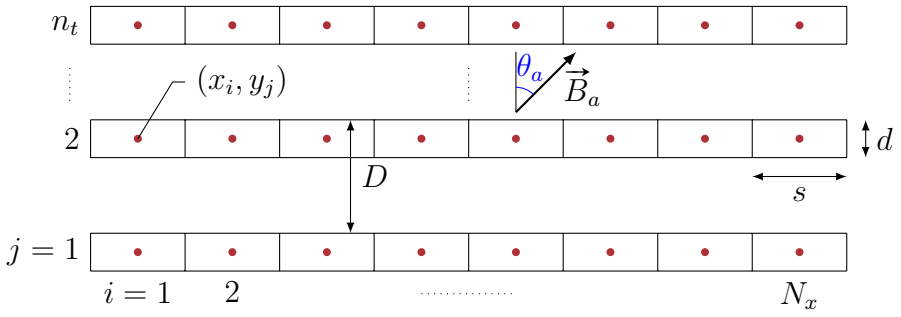

Fig. 1: Sketch of the geometry and definitions used in the numerical model.

gauge. In order to find distribution of the corresponding induced currents in the stack ΔI_k ($k = 1 \dots N$), first the following functional (see eq. (27) in [11]) is minimized:

$$L(\Delta I) = \sum_{i=1}^{N} \left(\frac{\sum_{j=1}^{N} \frac{1}{2} C_{ij} \Delta I_j \Delta I_i + \Delta A_{a_i} \Delta I_i}{\Delta t} + \frac{E_c I_{c_i}^{\text{cell}}}{n+1} \left(\frac{|I + \Delta I|}{I_c^{\text{cell}}} \right)_i^{n+1} \right) \tag{1}$$

where the power law current-voltage relation is used with the exponent n and $E_c = 1\,\mu\text{V/cm}$; $I_c^{\text{cell}} = j_c(B, \theta) \cdot s \cdot d$ is the critical current of the cell element being a function of the magnitude and direction of the magnetic field (at a given temperature); C_{ij} is the matrix of mutual inductances of the cell elements, which can be calculated analytically (see Appendix). Note that the original definition of L contains a term related to the transport current source ($\nabla\phi$ in eq. (27) of [11]) that has been dropped in the equation (1). We implement this term as a minimization constraint on ΔI: sum of the induced currents in the stack should be equal to the applied ramp of the transport current ΔI_{tr}. Note that using the gradient of L (see Appendix) provides more effective solving of the optimization problem.

After the minimization of L is completed, the obtained solution ΔI (i.e. intermediate distribution of the induced currents) is used to calculate the total magnetic field $\vec{B} = \vec{B}_a + \vec{B}_{\text{sf}}$, $\vec{B}_{\text{sf}} = \{M_x, M_y, 0\}(I + \Delta I)$ (see Appendix). In turn, it allows updating the critical currents of the cell elements and repeating the minimization of L. After several iterations the final distribution of the induced currents ΔI is obtained that ensures consistency between the total magnetic field and critical currents of the elements (within a given tolerance). Thus, the current distribution of the stack reads as $I(t + \Delta t) = I(t) + \Delta I$ and one can start the calculation of the induced currents ΔI for the next time step. Diagram of the described procedure of the calculation is illustrated in figure 2.

For the each considered time step we calculate the magnetic moment of the stack m and instantaneous power loss P as follows (both – per unit length of the stack):

$$\begin{aligned} m(t) &= \sum_{k=1}^{N} x_k I_k(t) \\ P(t) &= \sum_{k=1}^{N} E_k(t) I_k(t) = \sum_{k=1}^{N} \frac{E_c}{(I_{c_k}^{\text{cell}})^n} |I_k(t)|^{n+1} \end{aligned} \tag{2}$$

Finally, we calculate the hysteresis loss per cycle using the general expression: $Q = \oint P(t)\,\mathrm{d}t$. For the considering zero transport current case, one can also calculate

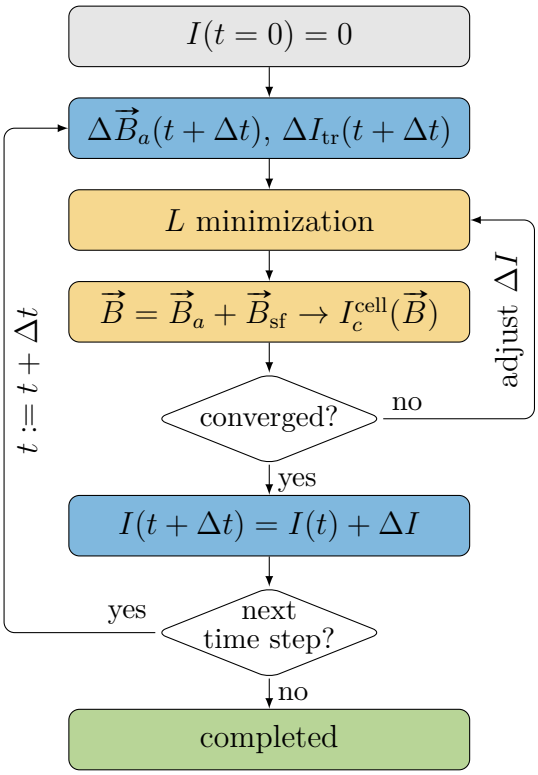

Fig. 2: Scheme of the numerical model.

the magnetization loss of the stack from the area of the corresponding magnetization loop (see [12] for the details): $Q = \oint m\,\mathrm{d}B_a$.

2.2. Benchmarking

The presented numerical model was benchmarked against several analytical solutions for the magnetization behavior of a single tape. For instance, results of the modeling with the parameters $n_t = 1$, $w = 4\,\mathrm{mm}$, $N_x = 100$, $j_c(B,\theta) = 40\,\mathrm{kA/mm^2}$ (field independent; $I_c^{\mathrm{cell}} = 1.6\,\mathrm{A}$), $n = 1000$ are presented together with the thin film behavior in the critical state model (see section III in [13]) in figure 3. Note that the curves in the left plot are marked with the values of time that correspond to the field ramp in the right plot. Due to an accurate agreement between the numeric data and Brandt's solution, we concluded a correct implementation of the model for high n-values. Additional validation of the n-value in the model was successfully performed by considering a saturated state of the tape, which also can be expressed analytically (see section V in [14]).

It turns out that the effect of the geometry on the modeling results is practically negligible already for $N_x \geqslant 30$. In order to decrease the computational time, $N_x = 30$ is retained for all the numerical results presented below.

2.3. Stack of tapes in the critical state model

There are two limit cases for the magnetization of the stacks in the perpendicular magnetic field (to the tape's face) that are solved analytically in the critical state model (i.e. assuming field independent j_c with $n \to \infty$): Brandt's solution for the single tape

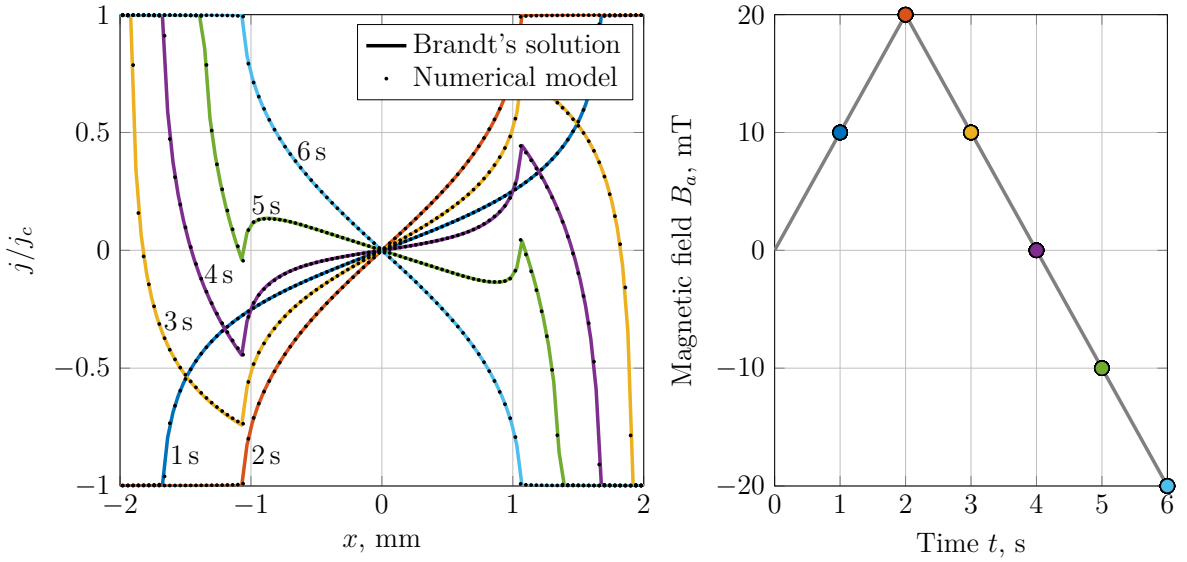

Fig. 3: Left: analytical (solid lines) and numerical (dots) results for the current distribution in a single 4-mm width tape. The curves are labeled with the values of time. Right: applied magnetic field as a function of time.

($n_t = 1$) [13] and Mawatari's solution for the stack with infinite number of tapes ($n_t = \infty$) [15]. These solutions can be expressed for the magnetization loss per volume per cycle (in J/(m^3·cycle)) as follows:

$$\begin{aligned} Q_{\text{brandt}} &= w j_c B_c q_1\left(B_a/B_c\right) \\ Q_{\text{mawatari}} &= w j_c B_c q_\infty\left(B_a/B_c, 2D/\pi w\right) \\ B_c &= \frac{\mu_0 j_c d}{\pi} \\ q_1(x) &= 2\ln(\cosh x) - x\tanh x \\ q_\infty(x,a) &= a^2\int_0^x (x-2\xi)\ln\left(1+\frac{\sinh^2(1/a)}{\cosh^2\xi}\right)\mathrm{d}\xi \end{aligned} \tag{3}$$

where the parameters definition is the same as used in the numerical model. Note that for the stacks with $D \gg w$ the Mawatari's solution converges to the Brandt's one: $q_\infty(x, a \gg 1) = q_1(x)$; for $D \ll w$ – to the slab solution: $q_\infty(x, a \ll 1) = q_{\text{slab}}(x, a) = a^2x^3/3$, if $x \leqslant 1/a$; $x - 2/(3a)$, if $x > 1/a$.

Using the numerical model, magnetization loss for the stacks with finite number of tapes n_t can be also calculated. Results of the calculation for the different n_t normalized by the Brandt's solution are presented in figure 4. The curves demonstrate gradual decrease of the loss with increasing n_t, that represents the effect of the magnetic shielding in the stack.

By taking into account a similar shape of the curves in figure 4, the following approach is used to parametrize the numerical results: one can consider the n_t-tape stack as the stack with infinite number of tapes but with some effective distance between the tapes $D_{\text{eff}}(n_t)$. Applying the valid limits for this parameter: $D_{\text{eff}}(\infty) = D$ and $D_{\text{eff}}(1) = \infty$, the obtained analytical parametrization for the magnetization loss reads

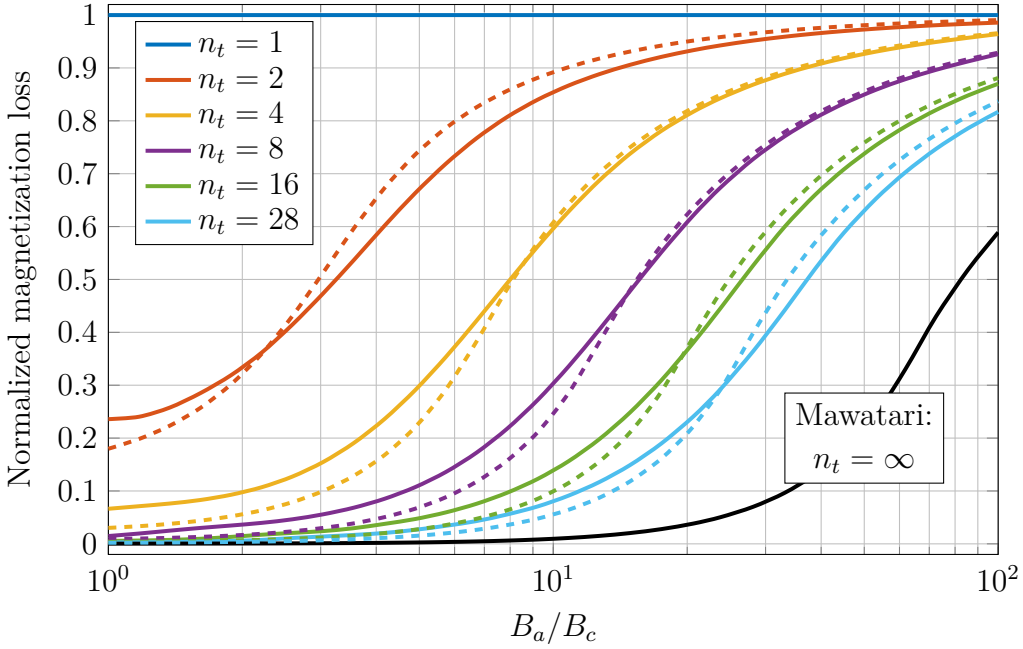

Fig. 4: Magnetization loss for the stacks with various number of tapes n_t in the critical state model normalized by the Brandt's solution (3). Solid lines represent the modeling results; dashed lines correspond to the proposed analytical approach in eq. (4).

as:

$$\begin{aligned} Q_{n_t} &= w j_c B_c q_{n_t}\left(B_a/B_c, 2D/\pi w\right) \\ q_{n_t}(x,a) &\approx q_\infty\left(x, a + \frac{0.34a^{0.10}}{n_t^{4.44a+0.65}-1}\right) \end{aligned} \tag{4}$$

The selected parametrization of the numerical results (see the dashed lines in figure 4) provides a quite accurate data representation, with the maximum deviation $\lesssim 5\,\%$.

3. Samples for the VSM measurements

The parameters of the stack samples that were prepared for the VSM measurements are summarized in table 1. Length of the sample should not exceed 10 mm due to a restricted volume of the VSM system at ENEA. SuperPower single tapes with different lengths (4 mm, 5 mm and 10 mm) and SuperPower 16-tape stacks (5 mm and 10 mm) can be used to verify an edge effect of the short samples. With the SuperPower 4-mm wide, 5-mm long stack samples the magnetic shielding and field's orientation effects with the varied number of tapes are studied. The list of samples allows also evaluating the influence of the tape's manufacturer on the magnetization behavior by comparing the SuperPower and SuperOx single tapes and 16-tape stacks. Note that there are no artificial pinning centers in the SuperOx tapes, while BZO doping is used by the SuperPower company. Finally, the geometry aspect ratio of the stack was included in the program by the SuperPower stacks of different tape's width (3 mm vs 4 mm) and thickness: the 3 mm width tapes are 60 µm thick, while all the other tapes are 100 µm thick.

Table 1: Description of the samples used in the VSM measurements.

HTS tape	Number of tapes, n_t	Orientation of the sample, θ_a
SuperPower width 4 mm length 4 mm	1	0°
SuperPower width 4 mm length 5 mm	1	0° / 45°
	8	0° / 45°
	16	0° / 45° / 90°
	28	0° / 45°
SuperPower width 4 mm length 10 mm	1	0°
	16	0°
SuperPower width 3 mm length 5 mm	1	0°
	8	0°
	16	0°
	28	0°
SuperOx width 4 mm length 5 mm	1	0°
	16	0°

All the stacks were assembled using the soldering device presented in figure 5. Short sections of tapes are stacked in the central groove of the bottom block (4 mm wide) and pressed by the top block. Then the device is heated by two heaters up to 200 °C controlling the temperature by a thermocouple inserted in the bottom block. During the melting of the solder additional pressing force is applied to ensure a tight packing of the stack. In case of the 3 mm width tapes, a narrower top pressing block is used with a teflon spacer to fill the width of the groove.

After the stack is soldered, the tapes in the stack are nicely packed in the cross-section, but slightly misaligned in the longitudinal direction. Because of that, slightly longer sections of tapes have been used in the soldering. The extra length from the misaligned edges of the stacks is cut away by the wire erosion, leading to a satisfactory geometry of the samples.

Cross-sections of the SuperPower stacks of 3 mm and 4 mm wide tapes are presented in figure 6. Presumably, a noticeable geometry artifact of the narrower stacks (parabolic shape of tapes at the bottom of the stack) is due to the bent surface of the pressing block. Since the solder thickness between the tapes is negligible, the distance between the tapes (i.e. parameter D of the numerical model, see previous section) reduces simply to the tape's thickness: 100 µm and 60 µm for the 4 mm and 3 mm width samples respectively.

For the samples assembling only 3 different spools with the tapes (production

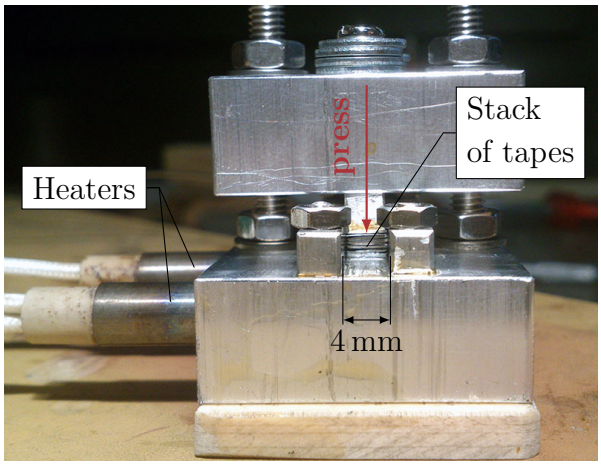

Fig. 5: Device for the stack soldering. A thermocouple is inserted at the rear side of the bottom aluminum block to control the heaters.

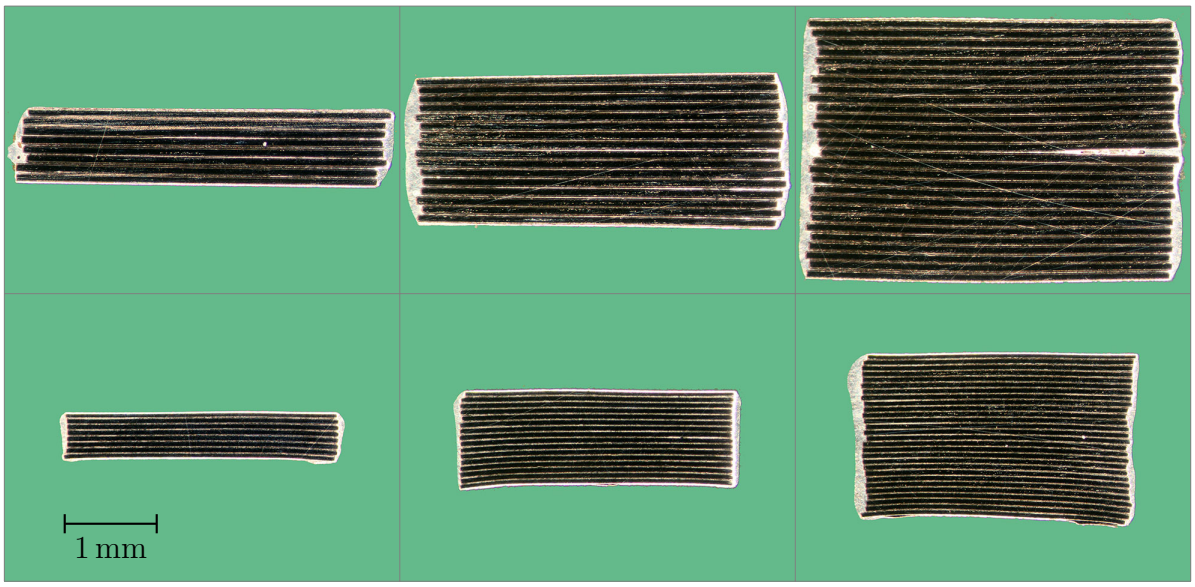

Fig. 6: Cross-sections of the SuperPower tape stacks. Columns from left to right: 8, 16 and 28-tape stacks. Dimensions of the tapes: 4 mm × 0.1 mm in the top row; 3 mm × 0.06 mm in the bottom row.

Table 2: I_c and n-value at 77 K / self-field of the tapes used for the samples manufacturing.

HTS tape	I_c, A	n-value
SuperPower 4 mm	155 ± 2	33
SuperPower 3 mm	70 ± 1	29
SuperOx 4 mm	164 ± 1	34

batches) are used: SuperPower-4mm, SuperPower-3mm and SuperOx-4mm. Before assembling, the critical currents and n-values of the tapes were measured in liquid nitrogen bath; see results in table 2.

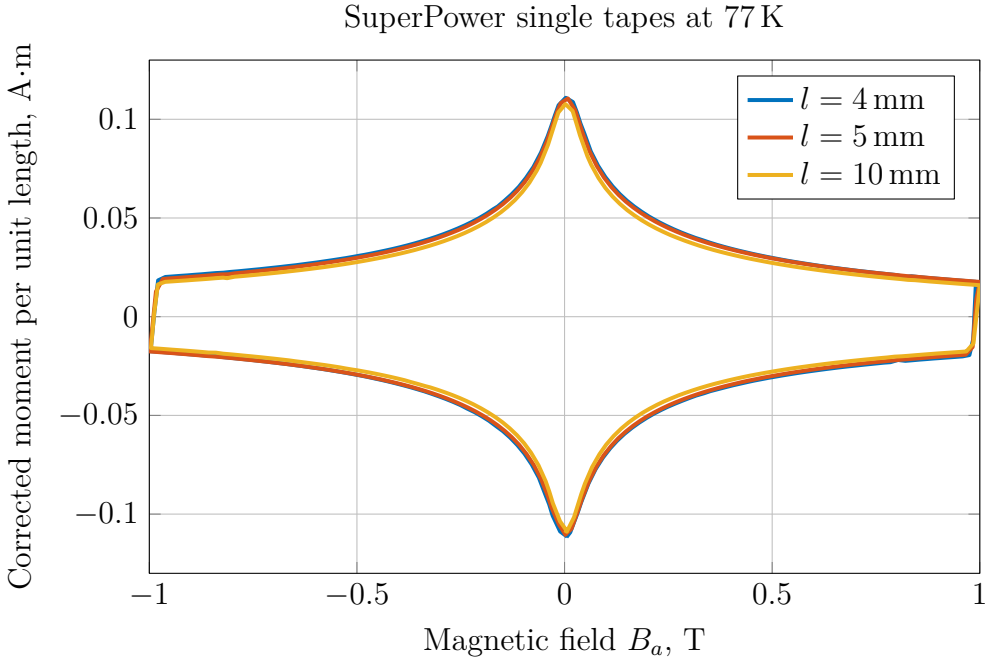

Fig. 7: Measured negative magnetic moment per unit length scaled by the finite length factor $(1 - w/3l)$ for the SuperPower 4 mm-width single tapes of different lengths l at 77 K.

4. Experimental results

4.1. Finite length effect

The magnetic moment of the stack samples is strongly influenced by the finite length and n-value of the tapes. For a single tape, the influence of each factor can be expressed analytically: the impact of the edge currents on m was considered in [16]; solution for the saturated state of the tape with finite n-value was given in [14]. Combining the both methods together, one can express m for the single tape as follows:

$$\frac{m_{\mathrm{sat}}}{l} = \frac{1}{4} I_c w \left(1 - \frac{w}{3l}\right) \left(\frac{\dot{B} w}{2E_c}\right)^{1/n} \frac{2n}{2n+1} \tag{5}$$

In the VSM measurements an effect of the ramp rate $\dot{B}$ on m was observed, which will be further discussed in [17]. To validate the finite length factor, the measured m is scaled by $(1 - w/3l)$ for the 4 mm-width single tapes of the different length: 4, 5 and 10 mm (see table 1). The results of the scaling at 77 K are presented in figure 7. From the transport measurements, the difference in I_c of these samples is negligible at 77 K. The scaling is also applied to the 16-tape SuperPower stacks (5 and 10 mm long) with the same satisfactory agreement. Thus, the scaling is justified and will be used further in this paper to obtain the magnetization behavior of long stacks from the short samples measurements.

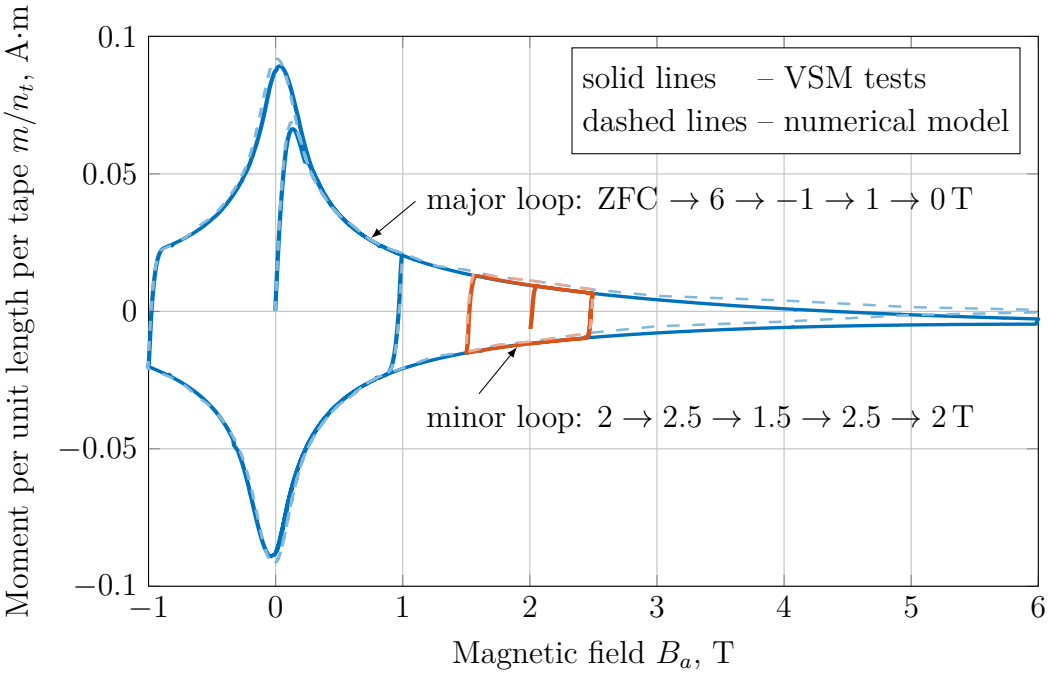

Fig. 8: Negative magnetic moment per unit length for the SuperOx 16-tape stack at 77 K.

4.2. Magnetization loops

The magnetization behavior of the stack samples described in table 1 was measured in the VSM system at 77 K and 5 K. For the measurements of the major magnetization loops the samples were cooled in zero field (ZFC), then the magnetic field was ramped as follows: ZFC → 6 → −1 → 1 → 0 T at 77 K; ZFC → 12 → −2 → 2 → 0 T at 5 K. In the minor loops measurements the field ramp was defined as 2 → 2.5 → 1.5 → 2.5 → 2 T at 77 K; 10 → 11 → 9 → 11 → 10 T at 5 K and performed at various ramp rates: 0.1, 0.2, 0.4, 0.6, 0.8 and 1.0 T/min. The minor loops are used to calculate the magnetization loss of the samples that will be discussed in the following section.

An example of major and minor loops of the SuperOx 16-tape stack at 77 K together with the corresponding modeling results is presented in figure 8. The angular dependence of the critical current $j_c(B, \theta)$ of the SuperOx tape at 77 K, used in the modeling, corresponds to the data presented in [18] and was provided by authors of that article in the tabulated form. Due to a weak influence of the n-value on the calculation for $n \gtrsim 15$, a constant n is retained as in table 2. Note that the developed numerical model (see previous section) has an accurate representation of the experimental data if the material properties are well defined.

Major magnetization loops for the SuperPower stacks with the different number of tapes n_t at 5 K are summarized in figure 9. The overlapping of the curves in the high field zone ($B \gtrsim 6$ T) suggest that the stack samples were not damaged during the assembly process. In the low field zone the self-field of the stacks has a strong impact on the resulting magnetic moment: the induced currents in the outer tapes of the stack generate sufficient magnetic field to ensure the shielding effect for the inner tapes. As a result, the magnetization loops become 'smoother' with the increasing number of tapes

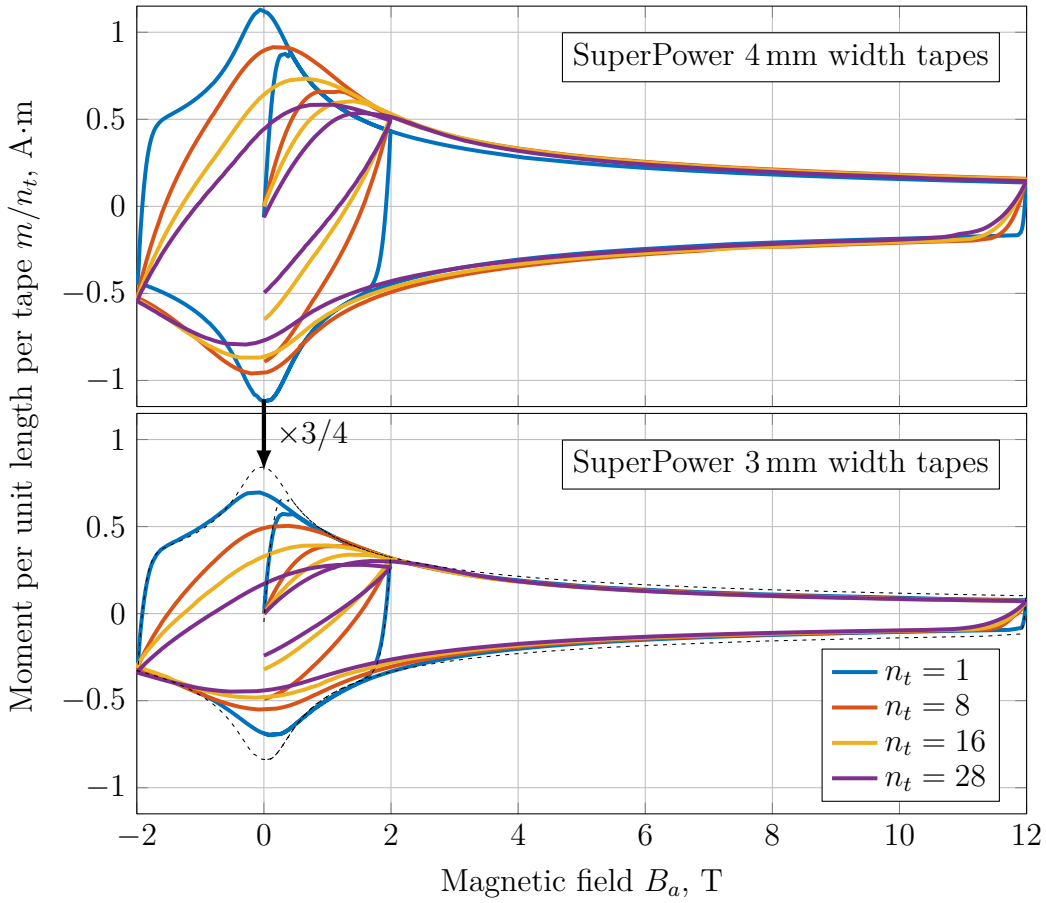

Fig. 9: Negative magnetic moment per unit length normalized by the number of tapes n_t for the SuperPower 4 mm and 3 mm width stacks at 5 K.

n_t. The bottom plot of figure 9 contains also the comparison between the loops of the single tapes of the different widths, which demonstrates a weaker I_c field dependence of 4 mm width tapes.

4.3. Orientation of the magnetic field

In order to apply the background magnetic field at $\theta_a = 45°$ and 90° to the c-axis of tapes, appropriate VSM sample holders were manufactured, see sketch in figure 10. Let assume that the resulting magnetic moment consists of the components, which are induced by the perpendicular ($\vec{B}_\perp$) and parallel ($\vec{B}_\parallel$) projections of the field with respect to the tape's face. The component of magnetic moment induced by $\vec{B}_\perp$ ($\vec{B}_\parallel$) is proportional to the tape's width w (tape's thickness d). Thus, due to a very high aspect ratio of the superconducting layer in the HTS tapes ($w/d \gtrsim 10^3$), the magnetic moment induced by the field with non-zero $\vec{B}_\perp$ (i.e. $\theta_a \neq 90°$) is directed essentially along the c-axis. As a consequence, an acting torque $\vec{\tau} = \vec{m} \times \vec{B}_a$ on the sample should be taken into account by an appropriate reinforcement of the sample's support. The main effect of $\vec{B}_\parallel$ on the magnetization is the reduction of the critical current due to that component, what in turn reduces the area of the loop.

A comparison of the magnetization loops for the SuperPower single tape at 5 K

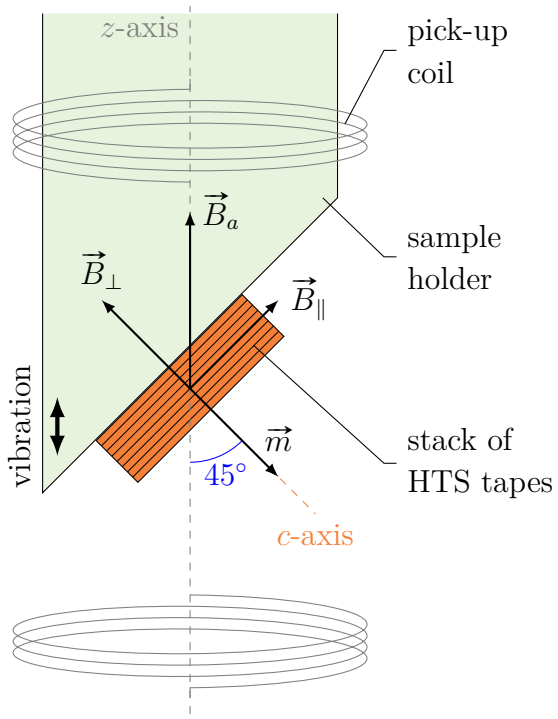

Fig. 10: VSM sample holder for the field orientation $\theta_a = 45°$ with respect to the c-axis of tapes. The electromotive force induced on the pick-up coils is proportional to m_z.

for 0° and 45° applied magnetic field is given in figure 11. For the 45° case, m versus $B_\perp$ is also presented, which was obtained from the measurements as $m = m_z/\cos\theta_a$, $B_\perp = B_a \cos\theta_a$ (see figure 10). This transformation preserves the area of the loop and consolidates the conclusions that has been done above: in the presence of $\vec{B}_\parallel$ component the loop is similar to the one in 0° applied field, but slightly squeezed (see also [19, 20]). For the 90° orientation reliable results could not be obtained in the VSM system due to a weak magnetization of the sample. SQUID magnetometer should be used instead as a more sensitive technique.

5. Magnetization loss

Using the minor loops measurements the magnetization loss of the stacks (see description in table 1) is calculated at 5 K and 77 K as an area of the closed loop: $Q = \oint m \, \mathrm{d}B_a$. A minor effect of the ramp rate on the loss was found and could be expressed as $Q \sim \dot{B}^{1/n}$ [21]. This relation can be simply obtained from the equation (5) if the sample is considered only in the saturated state (good assumption for the samples with a low penetration field).

The loss estimate as a function of the number of tapes n_t normalized by the loss of the single tape in the perpendicular field is summarized in figure 12 for both temperatures. The effect of the magnetic field shielding by the tapes' stacking results in the reduction of the loss with increasing number of tapes n_t. The same 20 % reduction was obtained for the SuperPower and SuperOx 16-tape stacks, what demonstrates a negligible influence of the tape's manufacturer. For the 4 mm and 3 mm width SuperPower stacks the difference

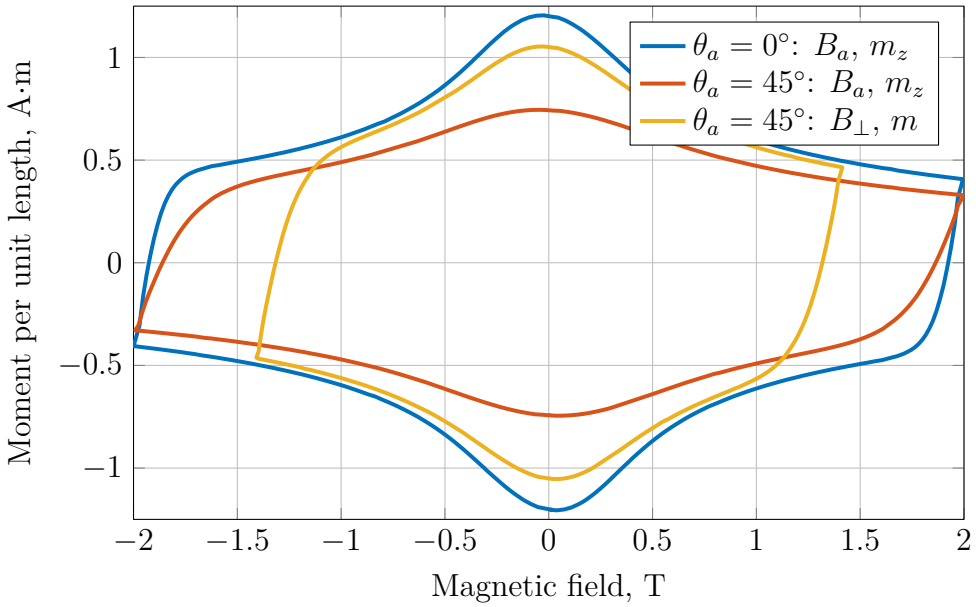

Fig. 11: Magnetization loops of the SuperPower single tape at 5 K for different orientations of the applied magnetic field. For the 45° applied field the loop in transformed coordinates is also presented.

in results is in agreement with the analytical expression (4): a lower aspect ratio D/w leads to lower loss (D/w is 0.025 and 0.020 respectively).

A further reduction of the loss was obtained in the field applied at 45° to the c-axis of the SuperPower stacks. In the measurements at 5 K the field ramp 10 ± 1 T corresponds to a variation of the perpendicular and parallel components by 7.1 ± 0.7 T. These variations are high enough to saturate the single tape: the 33 % loss reduction is mainly due to the shorter field ramp. In contrast, the full saturation was not achieved on the other samples, which have penetration field higher than 0.7 T: starting the loop from the upper branch of the magnetic moment, the bottom one was not reached in these measurements. As a result, the loss is additionally lowered by the weak magnetization of the stack samples.

Similar results were obtained at 77 K (right plot in figure 12), but the data are less smooth because of low absolute values of the loss ($\sim$30 times smaller than at 5 K). Note that the influence of the number of tapes n_t on the loss reduction at 77 K is much weaker than at 5 K. This can be explained by a low penetration field of the samples compared to the applied minor loops 2.0 ± 0.5 T. The tapes in the stack behave almost independent from the each other. The loss reduction for 45° oriented field ($\approx$ 30 %) correspond mainly to the shorter field ramp of the perpendicular field component, which is 29 % shorter than the one for the 0° case.

The solid lines in figure 12 represent the magnetization loss obtained from the developed numerical model (see section 2): the darker/lighter curve correspond to 0°/45° applied field respectively (for the both temperatures). At 5 K the modeling results correspond to the SuperPower tapes ($j_c(B, \theta)$ from [2]); at 77 K – to the SuperOx tapes ($j_c(B, \theta)$ from [18]). In case of 45° applied field at 5 K, the progressing deviation between the experimental and numerical data may be due to the discrepancy between the real and modeled angular dependence of the material. In this case, the full saturation was

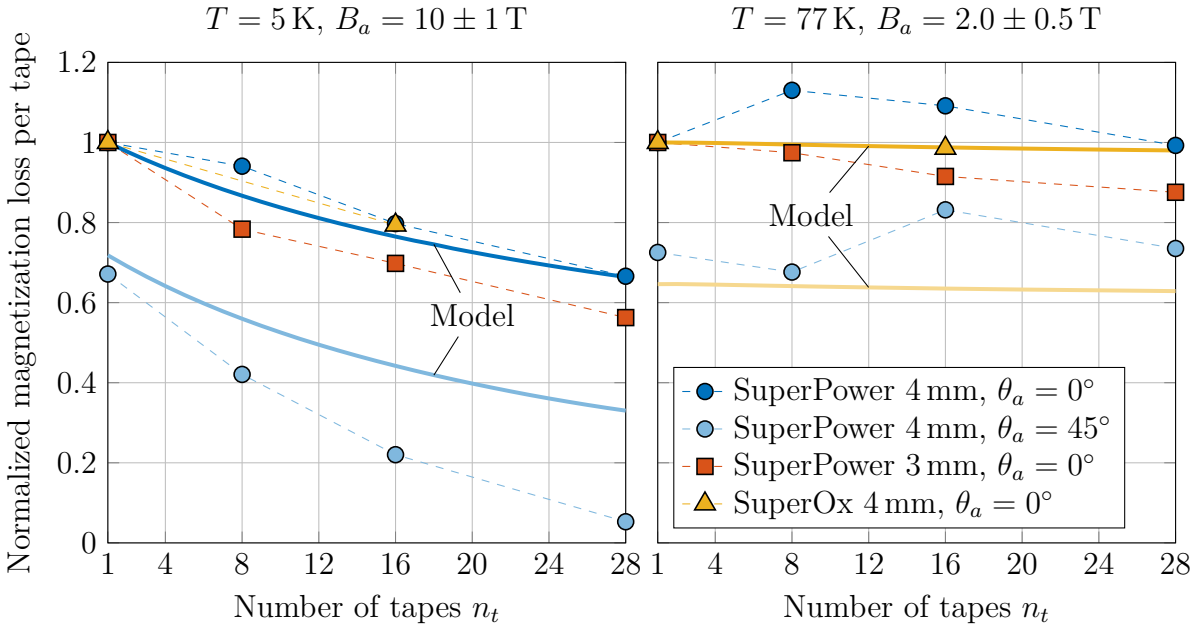

Fig. 12: Magnetization loss of the stacks per tape as a function of number of tapes n_t normalized to the single tape loss in the perpendicular field.

Table 3: Loss comparison for 16-tape stacks in the applied loop $2.0 \pm 0.3\,\mathrm{T}$ at 5 K.

Data source	Loss per tape, mJ/m/cycle	
	SuperPower	SuperOx
AC tests in EDIPO	from 13 to 30	
Numerical model	14.8	14.0
Analytical approach	12.7	11.2

not obtained also in the modeling for $n_t > 8$ (loops are not closed). In other cases there is a good correlation between the measurements and modeling.

The magnetization loss of the 16-tape stacks was estimated from the calorimetric AC loss tests performed with the 60 kA HTS cable prototypes in EDIPO [2, 3]. The AC loss of the SuperPower and SuperOx prototypes was measured against the frequency of the AC field from 0.1 Hz to 2 Hz, that allows assessing the magnetization loss by extrapolation to 0 Hz. Twisting of the stacks in the cables was accounted in the calculations in a simplified way: the loss was calculated as a function of field's orientation θ_a and then averaged over that parameter. The results obtained from the EDIPO tests, numerical simulation and analytical approach (see equation (4)) for the applied loops $2.0 \pm 0.3\,\mathrm{T}$ at 5 K are compared in table 3. For the SuperPower/SuperOx single twisted tape, the corresponding loss is estimated to $\approx 250\,\mathrm{mJ/m/cycle}$. According to the qualitative data agreement, the proposed analytical approach is also validated and can be used as a fast and reliable tool to estimate the magnetization loss of the stacked tapes.

6. Summary

Various aspects of the magnetization phenomena in the stacked HTS tapes have been studied from the numerical and experimental points of view. The developed numerical model served as an effective tool to propose the analytical approach for estimating the magnetization loss in the stacks with arbitrary number of tapes n_t and to better understand the underlying mechanisms of the magnetization. Using the VSM various aspects have been investigated, affecting the magnetization of the stacks: finite length and D/w aspect ratio effects, shielding of the magnetic field in the stacked tapes, orientation of the magnetic field with respect to the c-axis of the stack, influence of the temperature. A satisfactory agreement for the magnetization loss obtained from the modeling and measurements (including AC tests performed in the EDIPO test facility) has been demonstrated. This allows using the developed numerical tools in the performance assessment of next HTS cable prototypes. Further numerical tasks will address the implementation of the transport current term in the model and possible improvements in the optimization algorithms, since an appropriate selection of the solver may drastically speed up the calculation.

Acknowledgment

The authors would like to thank the Paul Scherrer Institute (PSI) for the technical support, Sandro Chiarelli and Ferruccio Maierna for providing the sample holders for VSM. N. Bykovsky also would like to express his gratitude to Enric Pardo for helpful advices regarding the numerical modelling, to Nikolay Mineev for the provided material properties of the SuperOx tapes at 77 K and to Giordano Tomassetti for suggesting advanced optimization algorithms.

This work has been carried out within the framework of the EUROfusion Consortium and has received funding from the Euratom research and training programme 2014-2018 under grant agreement No 633053. The views and opinions expressed herein do not necessarily reflect those of the European Commission.

Appendix

Vector potential in Coulomb's gauge and magnetic field generated by a current element that has uniform distribution of the current I and the rectangular bar geometry centred at the origin (infinitely long in z-direction, with s and d dimensions in xy-plane) can be expressed as:

$$\begin{aligned} \vec{A}(x,y) &= \frac{\mu_0 I}{4\pi s d}\{0,0,-z(f)\} \\ \vec{B}(x,y) &= \frac{\mu_0 I}{4\pi s d}\{-z(g_x), z(g_y), 0\} \end{aligned} \tag{A1}$$

where the functions f, g_x, g_y and functional operator z have the following definitions:

$$
\begin{aligned}
z(h) =& h_{(1,1)} - h_{(-1,1)} - h_{(1,-1)} + h_{(-1,-1)} \\
h_{(p,q)} =& h(x + p \cdot s/2, y + q \cdot d/2) \\
f(u,v) =& -3uv + uv \log(u^2+v^2) + u^2 \arctan\frac{v}{u} + v^2 \arctan\frac{u}{v} \\
g_x(u,v) =& u \log(u^2+v^2) + 2v \arctan\frac{u}{v} \\
g_y(u,v) =& g_x(v,u)
\end{aligned}
\tag{A2}
$$

Considering the two identical current elements centred at the positions (x_1, y_1) and (x_2, y_2), average vector potential and magnetic field generated by the first element with the current I over the cross-section of the second one can be obtained by direct integration of (A1) and reads as:

$$
\begin{aligned}
\langle\vec{A}\rangle(\Delta x, \Delta y) &= \frac{\mu_0 I}{4\pi s^2 d^2}\{0, 0, -Z(F)\} \\
\langle\vec{B}\rangle(\Delta x, \Delta y) &= \frac{\mu_0 I}{4\pi s^2 d^2}\{-Z(G_x), Z(G_y), 0\}
\end{aligned}
\tag{A3}
$$

where $\Delta x = x_2 - x_1$, $\Delta y = y_2 - y_1$. The functions F, G_x, G_y and functional operator Z have the following definitions:

$$
\begin{aligned}
Z(H) =& 4H_{(0,0)} + H_{(1,1)} + H_{(-1,-1)} + H_{(-1,1)} + H_{(1,-1)} - \\
& - 2(H_{(0,1)} + H_{(1,0)} + H_{(-1,0)} + H_{(0,-1)}) \\
H_{(p,q)} =& H(\Delta x + p \cdot s, \Delta y + q \cdot d) \\
F(u,v) =& -\frac{25}{24}u^2v^2 - \frac{1}{24}(u^4 + v^4 - 6u^2v^2)\log(u^2+v^2) + \\
& + \frac{1}{3}\left(u^3 v \arctan\frac{v}{u} + uv^3 \arctan\frac{u}{v}\right) \\
G_x(u,v) =& -\frac{1}{6}(v^3 - 3u^2 v)\log(u^2+v^2) + uv^2 \arctan\frac{u}{v} + \frac{1}{3}u^3 \arctan\frac{v}{u} \\
G_y(u,v) =& G_x(v,u)
\end{aligned}
\tag{A4}
$$

Hence, matrix of the mutual inductances of the current elements per unit length is written as $C = \langle\vec{A}\rangle/I$; matrices for the magnetic field components are written as $M_x = \langle\vec{B}\rangle_x/I$, $M_y = \langle\vec{B}\rangle_y/I$.

Finally, in order to increase the computational speed of the numerical model, the following expression for the gradient of functional L (see eq. (1)) can be used in the optimization methods:

$$
\frac{\partial L}{\partial \Delta I_i} = \frac{\sum_{j=1}^{N} C_{ij}\Delta I_j + \Delta A_{a_i}}{\Delta t} + E_c \operatorname{sgn}(I + \Delta I)_i \left(\frac{|I + \Delta I|}{I_c^{\text{cell}}}\right)_i^n
\tag{A5}
$$

From the physical point of view, this expression represents the electric field that drives the current redistribution.

References

[1] P. Bruzzone, B. Stepanov, D. Uglietti, R. Wesche, and K. Sedlak, "EDIPO: the test facility for High-Current High-Field HTS superconductors", IEEE Transactions on Applied Superconductivity **26**, 9500106 (2016).

[2] D. Uglietti, N. Bykovsky, K. Sedlak, B. Stepanov, R. Wesche, and P. Bruzzone, "Test of 60 kA coated conductor cable prototypes for fusion magnets", Superconductor Science and Technology **28**, 124005 (2015).

[3] N. Bykovsky, D. Uglietti, K. Sedlak, B. Stepanov, R. Wesche, and P. Bruzzone, "Performance evolution of 60 kA HTS cable prototypes in the EDIPO test facility", Superconductor Science and Technology **29**, 084002 (2016).

[4] F. Grilli, S. Ashworth, and S. Stavrev, "Magnetization AC losses of stacks of YBCO coated conductors", Physica C: Superconductivity **434**, 185–190 (2006).

[5] V. M. R. Zermeno, A. B. Abrahamsen, N. Mijatovic, B. B. Jensen, and M. P. Sorensen, "Calculation of alternating current losses in stacks and coils made of second generation high temperature superconducting tapes for large scale applications", Journal of Applied Physics **114**, 173901 (2013).

[6] E. Brandt, "Theory of type-II superconductors with finite london penetration depth", Physical Review B **64** (2001) 10.1103/PhysRevB.64.024505.

[7] I. A. Rudnev and A. I. Podlivaev, "Magnetic response of the stacks of HTS tapes", IEEE Transactions on Applied Superconductivity **26**, 1–4 (2016).

[8] L. Prigozhin and V. Sokolovsky, "Computing AC losses in stacks of high-temperature superconducting tapes", Superconductor Science and Technology **24**, 075012 (2011).

[9] E. Pardo, A. Sanchez, D.-X. Chen, and C. Navau, "Theoretical analysis of the transport critical-state ac loss in arrays of superconducting rectangular strips", Physical Review B **71** (2005) 10.1103/PhysRevB.71.134517.

[10] E. Pardo, "Modeling of coated conductor pancake coils with a large number of turns", Superconductor Science and Technology **21**, 065014 (2008).

[11] E. Pardo, J. Souc, and L. Frolek, "Electromagnetic modelling of superconductors with a smooth current-voltage relation: variational principle and coils from a few turns to large magnets", Superconductor Science and Technology **28**, 044003 (2015).

[12] F. Grilli, E. Pardo, A. Stenvall, D. N. Nguyen, Weijia Yuan, and F. Gomory, "Computation of losses in HTS under the action of varying magnetic fields and currents", IEEE Transactions on Applied Superconductivity **24**, 78–110 (2014).

[13] E. Brandt and M. Indenbom, "Type-II-superconductor strip with current in a perpendicular magnetic field", Physical Review B **48**, 12893–12906 (1993).

[14] E. H. Brandt, "Superconductors of finite thickness in a perpendicular magnetic field: strips and slabs", Physical Review B **54**, 4246 (1996).

[15] Y. Mawatari, "Critical state of periodically arranged superconducting-strip lines in perpendicular fields", Physical Review B **54**, 13215–13221 (1996).

[16] E. M. Gyorgy, R. B. van Dover, K. A. Jackson, L. F. Schneemeyer, and J. V. Waszczak, "Anisotropic critical currents in Ba2YCu3O7 analyzed using an extended bean model", Applied Physics Letters **55**, 283 (1989).

[17] G. De Marzi, G. Iannone, U. Gambardella, C. F. Zignani, and A. della Corte, "Magnetic losses in the Low-Frequency range of commercial REBCO coated conductors", to be presented at ASC (2016).

[18] N. Mineev and I. Rudnev, "Measurements and numerical simulations of trapped field in a stack of HTS tapes", IEEE Transactions on Applied Superconductivity **26**, 1–4 (2016).

[19] Y. Fukuda, K. Toyota, K. Kajikawa, M. Iwakuma, and K. Funaki, "Field angle dependence of AC losses in stacked Bi-2223/Ag sheathed tapes", IEEE Transactions on Applied Superconductivity **13**, 3610–3613 (2003).

[20] Z. Jiang, N. Amemiya, K. Kakimoto, Y. Iijima, T. Saitoh, K. Suzuki, and Y. Shiohara, "Total AC loss characteristics in a stacked YBCO conductor", IEEE Transactions on Applied Superconductivity **17**, 2442–2445 (2007).

[21] M. Polak, J. Kvitkovic, P. Mozola, E. Usak, P. N. Barnes, and G. A. Levin, "Frequency dependence of hysteresis loss in YBCO tapes", Superconductor Science and Technology **20**, S293–S298 (2007).